Multilayered Nanoheterostructures: Theory and Experiment

D. Dorfs, H. Henschel, J. Kolny, and A. Eychmüller*

Department of Physical Chemistry, University of Hamburg, Bundesstrasse 45, 20416 Hamburg, Germany

Received: September 4, 2003; In Final Form: October 29, 2003

A series of multilayered nanocrystals consisting of alternating CdS and HgS layers has been synthesized. Those structures have been characterized by UV/VIS/NIR absorption and emission spectroscopy as well as transmission electron microscopy. Results of the optical spectroscopy are compared to theoretical calculation ("effective mass approximation") and TEM results are compared to TEM simulations. Furthermore, comparable structures consisting of ZnS and CdS have been synthesized and characterized by optical spectroscopy and powder X-ray diffractometry.

Introduction

Multilayered nanocrystals have been the focus of scientific research almost since the beginning of colloidal synthesis of nanocrystals. Many so-called "core−shell" particles, consisting of a core and a shell of a different semiconducting material, are known today. The very first approach to this kind of structures by Spanhel et al.[1] dealt with CdS particles covered with $Cd(OH)_2$ in aqueous solution while a later organometallic approach, for example, by Peng et al.,[2] yielded CdSe nanocrystals covered with a shell of CdS. In these core−shell structures, the coating layer consists commonly of a material with a larger band gap than the core material resulting in a localization of the charge carriers in the core and thus increasing the photoluminescence quantum yield by passivating the surface of the particles.

Nanocrystals consisting of CdS with an embedded layer of HgS were first prepared by Mews et al.[3] Because of the smaller band gap of HgS compared to that of CdS, these structures were termed "quantum dot quantum well" (QDQW). In those "onionlike" structures, a strong localization of the charge carriers within the embedded HgS layer occurs. These structures were subsequently intensively investigated with different types of optical spectroscopy,[4−11] with high-resolution transmission electron microscopy,[12] and subsequently compared with theoretical calculations.[13−16] A comparable structure consisting of ZnS with an embedded layer of CdS has been synthesized and characterized using absorption spectroscopy by Little et al.[17] and the results were also compared with theoretical treatments.[17,18] The first step toward a more complicated structure with two embedded HgS layers inside a CdS nanocrystal was presented by Braun et al.[19] In an earlier letter,[20] we compared a series of similar nanoheterostructures in terms of their absorption spectroscopy and transmission electron microscopy. Recently, these structures were investigated with X-ray photoelectron spectroscopy (XPS) using tunable synchrotron radiation.[21]

Here, we present further characterizations of these kinds of "double well quantum dot" structures, using emission spectroscopy and TEM simulations. In addition, we compare our results with theoretical calculations performed within the framework of the effective mass approximation. For the remainder of the article, we describe the results of our effort to synthesize and characterize single-well ZnS/CdS/ZnS systems.

Experimental Section

Apparatus. Absorption spectra were measured in 1-cm quartz cuevettes using a Cary 500 spectrometer (Varian) at a spectral resolution of 1 nm. UV/vis emission spectra were recorded using a Fluoromax-2 spectrometer (Instruments S. A. Inc.). Low-temperature emission spectra were measured in the same instrument in combination with a closed cycle helium cryostat (Leybold), equipped with a top-loading unit. NIR emission spectra were measured with a Fluorolog spectrometer (Instruments S. A. Inc.) equipped with a liquid nitrogen cooled germanium detector. All emission spectra were measured in 1-cm quartz cuevettes, at a spectral resolution of 3 nm in the UV/vis emission spectra and 5 nm resolution for the NIR emission spectra.

For transmission electron microscopy (TEM), a small drop of the colloidal solution was dried on a carbon-coated copper grid. The images were obtained using a CM 300 UT transmission electron microscope (Phillips) at an acceleration voltage of 300 kV.

Powder X-ray diffractograms were recorded with an X'pert System (Phillips) using copper-K-radiation and a nickel filter for absorbing the K_β-radiation.

The simulation of the HRTEM images was performed at Scherzer focus using the HRTEM module of the software package Cerius2, version 4.0, running on an SGI Fuel workstation. The constructed model of a tetrahedral CdS particle (CdS particle with two embedded HgS layers) with bulk fcc structure has been placed for the simulation into a box with 12 nm × 16.5 nm × 16.5 nm cell dimensions.

Preparation. *CdS/HgS Systems.* The CdS cores were synthesized as described by Spanhel et al.,[1] by the injection of H_2S into an aqueous solution of $Cd(ClO_4)_2$ and Grahams salt ($Na_x(PO_3)_x$ where $x \approx 6$), yielding CdS particles of a mean diameter of 5.3 nm.

Figure 1 shows schematically the preparative route for different CdS/HgS/CdS/HgS/CdS QDQWs. CdS/HgS/CdS QDQWs with different layer thicknesses were prepared in a manner similar to that described by Mews et al.[4] An aqueous solution of $Hg(ClO_4)_2$ is added to a solution of the CdS particles which

* Address correspondence to this author. E-mail: eychmueller@chemie.uni-hamburg.de.

10.1021/jp036643t CCC: $27.50
Published on Web 01/10/2004

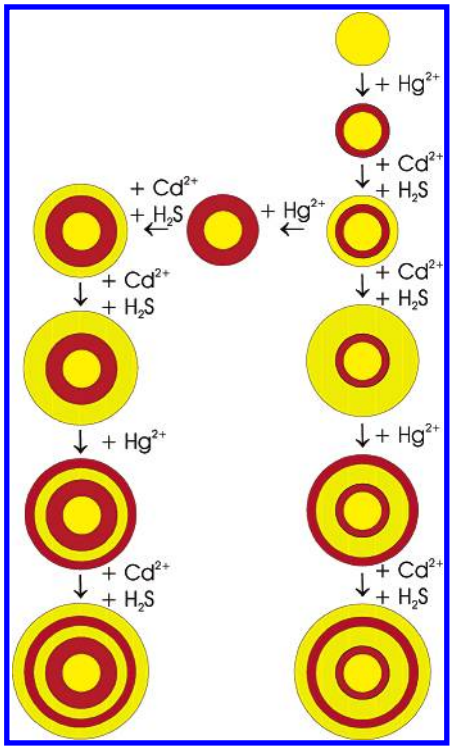

Figure 1. Synthetic route for different CdS/HgS structures.

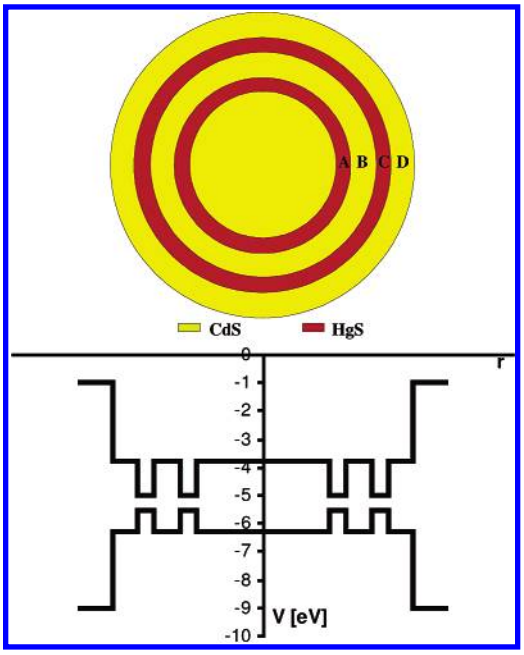

Figure 2. Idealized picture of the double well quantum dot structure with introduction of the CdS/HgS-ABCD nomenclature and the corresponding radial potential for electron and hole.

results in a substitution of the outermost CdS layer of the nanocrystals by HgS; subsequently, CdS layers are grown onto the particles by addition of the required amount of $Cd(ClO_4)_2$ (taking into account the Cd^{2+} ions released into the solution by the substitution reaction) and afterward by the slow injection of H_2S at a pH 5.5 (kept constant by dropwise addition of NaOH). As described in a previous letter,[20] CdS/HgS/CdS/HgS/CdS QDQWs with different layer thicknesses were prepared by repeating the substitution reaction described by Mews et al. with a CdS/HgS/CdS QDQW instead of a CdS particle. The amount of $Hg(ClO_4)_2$ or $Cd(ClO_4)_2$ and H_2S for the substitution of a monolayer of CdS by HgS or the growing of a CdS monolayer were calculated for each layer assuming spherical growth of the particles and a monolayer thickness of 0.3 nm.

ZnS/CdS Systems. ZnS nanocrystals were prepared by injecting 16 mL of H_2S into 800 mL of a degassed aqueous solution containing 3.2 mL of a 0.1 M $Zn(ClO_4)_2$ solution and 0.4 mL of a 0.1 M $Na_6(PO_3)_6$ solution at a pH value of 10.5 (adjusted with 0.1 M NaOH) under strong stirring. After 10 min, the pH value had dropped to 8.0 and the solution had been degassed until the pH value remained constant at 6.5. Then, the pH was adjusted to 7.0 by addition of 0.1 M NaOH.

For the substitution of the first monolayer of ZnS by CdS, 0.4 mL of a 0.1 M $Cd(ClO_4)_2$ solution (assuming spherical shape of the nanocrystals, a diameter of 3 nm and a monolayer thickness of 0.3 nm for both materials, this amount corresponds exactly to a thickness of one monolayer) was added to 200 mL of the solution of ZnS nanocrystals. The solution was then heated to 70 °C until no further shift to lower energies in the absorption spectrum is observed (approximately 2 h).

To grow cladding layers of ZnS on the nanocrystals, the required amount of $Zn(ClO_4)_2$ solution was added (calculated for each different layer with the same assumptions mentioned above and taking into account the assumed amount of Zn^{2+} ions released into the solution by the substitution reaction) and the pH value was adjusted to 6.0. Then, the required amount of H_2S (20% excess) was slowly injected and the pH value was constantly adjusted to 6.0 by dropwise addition of 0.1 M NaOH. Afterward, the pH value was again adjusted to 7. Systems with different layer thicknesses can be synthesized by repeating the substitution reaction and the cladding process analogue to the CdS/HgS/CdS systems.

Results and Discussion

CdS/HgS Systems. *Nomenclature*. For ease of discussion, all CdS/HgS/CdS/HgS/CdS samples are named according to Figure 2 as CdS/HgS-ABCD (see also ref 20), where each letter stands for the thickness of the corresponding layer in monolayers. Thus, for example, CdS/HgS-1213 relates to a nanocrystal consisting of a CdS core, followed by 1 monolayer of HgS, 2 monolayers of CdS, 1 monolayer of HgS, and again 3 monolayers of CdS. CdS/HgS/CdS and ZnS/CdS/ZnS QDQWs are analogously named as CdS/HgS-AB and ZnS/CdS-AB. Of course, this nomenclature refers to an idealized situation. In reality, the particles have variations in the thickness of all layers and are expected to have inhomogeneities within the different layers.

Theoretical Calculations. The radial wave functions and the corresponding eigenvalues for electron and hole for the different multilayered structures have been calculated using the "effective mass approximation" as described by Schooss et al.[13] for single-well particles and later by Xia et al. for double-well particles[22] with the radial potential shown in Figure 2. A correction term for the attractive coulomb interaction between electron and hole was calculated using the same equations as Schooss et al.[13] Thus, eigenvalues for electron and hole were calculated using the Schrödinger equation for a particle within a potential $V(r)$, where $V(r)$ is given as shown in Figure 2:

$$\hat{H}\psi(\vec{r}) = E\psi(\vec{r}) \text{ with } \hat{H} = -\frac{\hbar^2}{2m_{\text{eff}} \cdot m_e}\Delta + V(\vec{r})$$

In areas with $E > V$, the resulting radial wave function $R_q(r)$ is given by a linear combination of Bessel functions j and

Neumann functions n (where q is the index for the different layers).

$$R_q(r) = A_q j(k_q,r) + B_q n(k_q,r) \text{ with } k_q = \sqrt{\frac{2m_q(E - V_q)}{\hbar^2}}$$

In areas with $E < V$, the wave function is given by a linear combination of the Hankelfunctions $h^{(+)}$ and $h^{(-)}$.

$$R_q(r) = C_q h^{(+)}(\kappa_q,r) + D_q h^{(-)}(\kappa_q,r) \text{ with } \kappa_q = \sqrt{\frac{2m_q(E - V_q)}{\hbar^2}}$$

For a system of N layers, there are $2N$ coefficients to be calculated. Two of these are zero because the resulting wave function has to disappear for $r \rightarrow \infty$ and has to be finite for $r = 0$. Thus, only $2N - 2$ coefficients remain.

On each of the $N - 1$ layer interfaces, the two following conditions have to be met:[23]

$$R_q(r_q) = R_{q+1}(r_q)$$

$$\frac{1}{m_q}\frac{dR_q(r)}{dr}\bigg|_{r=r_q} = \frac{1}{m_{q+1}}\frac{dR_{q+1}(r)}{dr}\bigg|_{r=r_q}$$

The result is a homogeneous linear system of equations with $2N - 2$ equations and $2N - 2$ coefficients containing the eigenvalue E as a variable. The equation system has only a nontrivial solution when the corresponding determinant $D(E)$ disappears ($D(E) = 0$)). Thus, the eigenvalue of the system is given by the root of the determinant $D(E)$. All coefficients may then be expressed as a function of one of the coefficients which may be arbitrarily chosen. This remaining coefficient can be obtained by the normalization condition:

$$||\Psi||^2 = \int_0^\infty R^*(r)R(r)r^2dr = 1$$

Once the wave functions of the electron and hole are known, the coulomb interaction can be calculated as follows:

$$E_c = -\frac{e^2}{4\pi\epsilon_0}\int\int dr_{e^-}dr_{h^+}r_{e^-}{}^2 r_{h^+}{}^2 \frac{|R_{e^-}(r_{e^-})|^2|R_{h^+}(r_{h^+})|^2}{\max(r_{e^-},r_{h^+})}\frac{1}{\bar{\epsilon}_r(r_{e^-},r_{h^+})}$$

($\bar{\epsilon}_r(r_{e^-},r_{h^+})$ is the average dielectric constant between electron and hole, for details see ref 13.)

The first electronic transition is then given by the sum of the eigenvalues of electron and hole and the coulomb interaction.

$$E_{gap} = E_{e^-} + E_{h^+} + E_c$$

All physical constants needed for those calculations are shown in Table 1.

Figure 3 shows calculated radial probabilities of presence for the electron and the hole for the CdS/HgS-1x13 series of nanocrystals according to the nomenclature described above, where x is varied from $x = 0$ to $x = 7$. All those nanocrystals contain the same CdS core, two wells each consisting of one monolayer of HgS and three outer cladding layers of CdS, the only difference being the distance between the two HgS wells which is varied from zero to seven monolayers of CdS.

As expected, the probability of presence has a maximum within the HgS wells for both the electron and the hole, thus giving rise to a spatial overlap of the two wave functions within the HgS wells. Because of the higher effective mass of the hole compared to that of the electron in both materials, the localization is much stronger for the hole than for the electron in the same systems. Increasing the distance between two HgS monolayers results in a stronger separation of the two maxima of the probability of presence; thus, in the CdS/HgS-1713 system the two maxima of the probability of presence for the hole are almost totally separated from each other. This separation becomes more and more smeared out with a decrease in distance of the two HgS layers. Similar behavior is observed for the electron but because of the lower effective mass the maxima are not separated to the same degree even for the system with the largest distance between two HgS layers (i.e., CdS/HgS-1713).

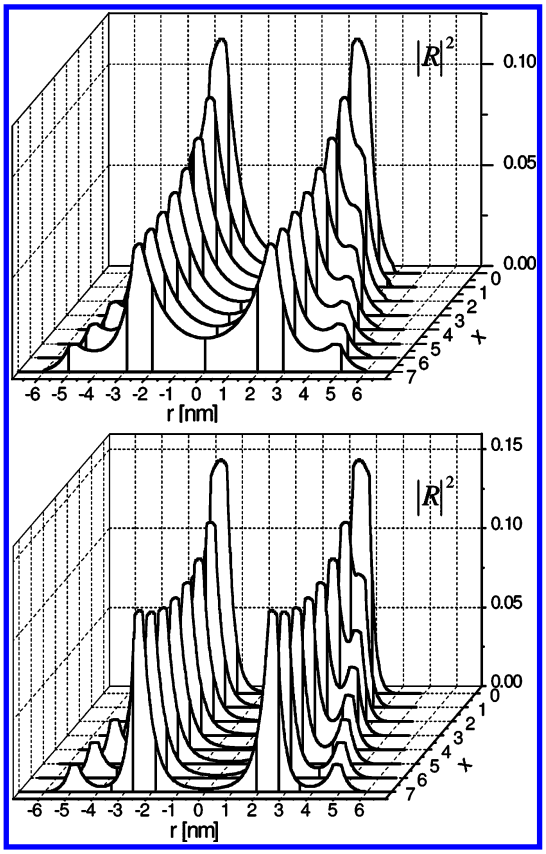

Figure 3. Radial probability of presence in the CdS/HgS-1x13 Systems ($x = 0-7$) for the electron (top) and the hole (bottom), r is the radial distance from the particle center.

TABLE 1: Physical Constants Used for the Theoretical Calculations

material	upper edge of valence band	band gap	$m_{eff}(e^-)$	$m_{eff}(h^+)$	ϵ
ZnS	−6.7 eV	3.7 eV	0.34	0.58	5.7
CdS	−6.3 eV	2.5 eV	0.2	0.7	5.5
β-HgS	−5.5 eV	0.5 eV	0.036	0.044	11.36

Spectroscopy. Figure 4 (left) shows the UV/vis-absorption spectra of the CdS/HgS-1x13 series of nanocrystals with $x = 0$ to $x = 4$. The vertical bars represent the calculated first electronic transition (E_{gap}) for the corresponding ideal system. In general, the point of maximum curvature is believed to represent the first electronic transition of a sample. For the samples CdS/HgS-23, CdS/HgS-1113, and CdS/HgS-1213, this point matches quite well with the calculated values. For the samples CdS/HgS-1313 and CdS/HgS-1413, such a point is difficult to discern but still the absorption onset of those samples is shifted toward higher energy which is in good agreement with the calculated values (cf. vertical bars). This may be explained by a decreasing interaction between the two HgS layers with increasing distance

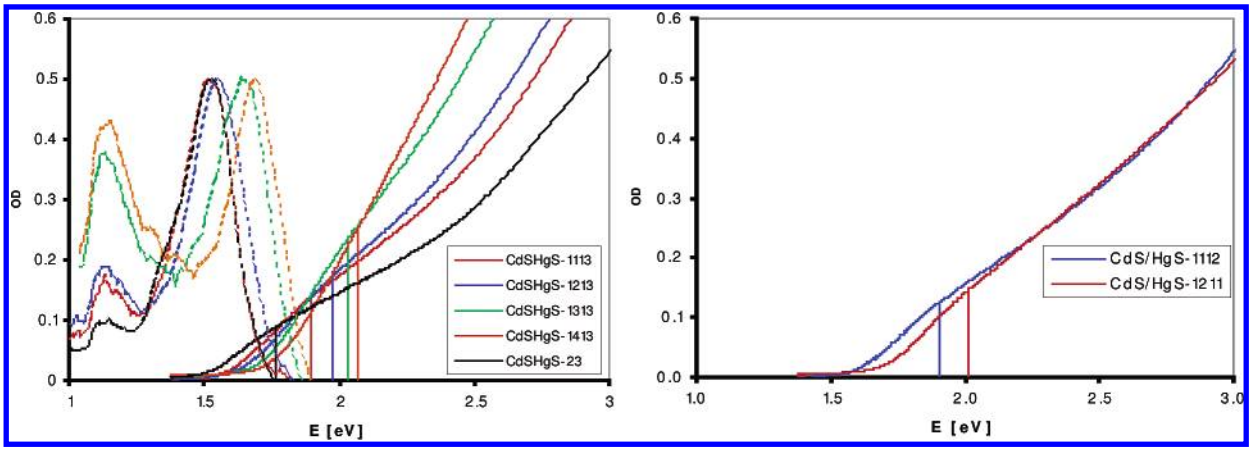

Figure 4. UV/vis-absorption and emission spectra (lines and dotted lines, respectively) of the CdS/HgS-1*x*13 systems together with the calculated eigenvalues of the first electronic transition (left) and the comparison of two systems with the same amount of CdS and HgS but different layer structure (right). Lines of the same color refer to the same sample in the left figure.

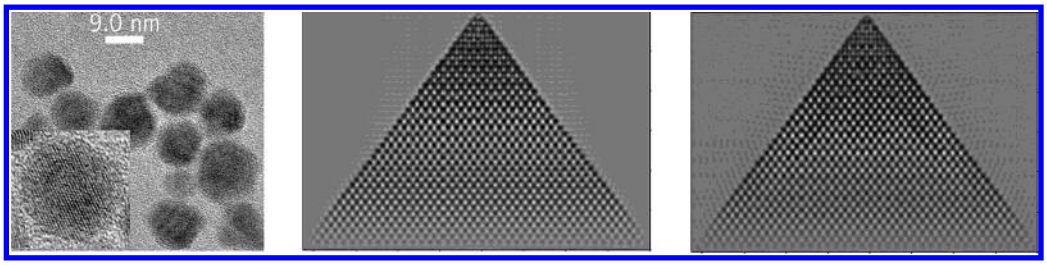

Figure 5. HRTEM picture (single particle in the inset to visualize the lattice planes) of the CdS/HgS-2223 system (left), TEM simulations of pure CdS nanocrystal (middle), and a double well quantum dot structure (right).

between those layers. The high energy absorption (above 2.5 eV) appears to depend mainly on the total amount of absorbing material. This is concluded from the experimental procedure: all samples were taken out of the crude reaction mixture and thus the particle concentration is assumed to be constant in all measurements and consequently we observe the systems with the thicker CdS layer between the HgS layers having a higher oscillator strength in this region. The absorption behavior between 1.8 and 2.2 eV is difficult to explain since the presented simple theoretical treatment is unable to explain the oscillator strengths in different regions of the spectra.

The dotted lines in Figure 4 (left) are the corresponding normalized emission spectra of these samples. Each sample shows an emission close to the band gap. The relative position of the emission maxima is in good agreement with the absorption onsets of the samples. Furthermore, each sample shows a second emission at 1.15 eV which is likely to be "trap-emission" because of stacking faults at the interfaces of the layers as previously shown by ODMR measurements on the CdS/HgS/CdS systems.[24] Emission quantum yields for the different systems were not determined but they are considered to be low. Assuming a defect-free structure, the emission quantum yields should depend on the overlap between electron and hole wave functions. Since the photoluminescence intensity in the real particles is most likely dominated by the amount of stacking faults and surface traps, a theoretical discussion of the photoluminescence intensity within the presented simple model seems to be inappropriate.

To show that the absorption onsets of those systems are not only affected by the molar ratio of CdS to HgS but indeed depends on the layer structure, Figure 4 (right) shows a comparison of two structures with the same molar ratio but a different layer structure (CdS/HgS-1112 and CdS/HgS-1211). The structure in which the HgS wells are separated by two monolayers of CdS and with a capping layer of one monolayer shows an absorption onset at higher energy compared to the system with a separation of one layer of CdS and two capping layers of CdS. In both cases, the agreement with the calculated transition energy (again given by the vertical bars) is satisfactory.

Transmission Electron Microscopy (TEM). As shown in a previous letter,[20] the particle growth during the different syntheses steps can be monitored by TEM measurements and the observed particle growth is in good agreement with the estimated structures.

Figure 5 (left) shows a high-resolution TEM image of the CdS/HgS-2223 sample which gives clear proof for the crystallinity of the sample (0.334-nm lattice spacing matching cubic CdS as well as β-HgS). But no indication of a layer structure can be found in this image. Figure 5 also shows TEM simulations of a pure CdS particle (middle) and a CdS/HgS-2223 nanocrystal to show whether a contrast difference for the different layers can be expected. For these simulations, we choose an idealized situation to make visible a contrast difference between the CdS and the HgS. Therefore, the particles have a tetrahedral shape, the embedded HgS facets are aligned parallel to the electron beam of the TEM, and no carbon grid is included in the simulations. Even under these perfect conditions, no contrast difference is discernible, from which it is concluded that in real images contrast differences are not expected to be observed.

ZnS/CdS Systems. *Spectroscopy.* Figure 6 shows the absorption spectra of all structures of the synthetic route leading to the ZnS/CdS-13 (left) and the ZnS/CdS-23 (right) systems. Again, the calculated values for the first electronic transitions are represented by the vertical bars (for the physical constants refer to Table 1). For all samples, the calculated values fit very well to the transitions observed in the recorded spectra. Since CdS has the smaller band gap, the shift to lower energies compared with the ZnS/CdS-1 system is easily understood. The shift to lower energies with enhanced thickness of the ZnS

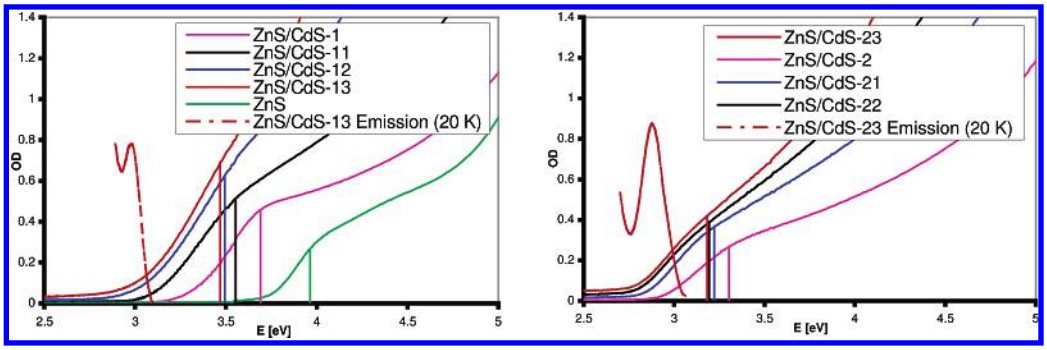

Figure 6. UV/vis absorption spectra of the ZnS-core, the ZnS/CdS-1x systems, and the ZnS/CdS-2x systems.

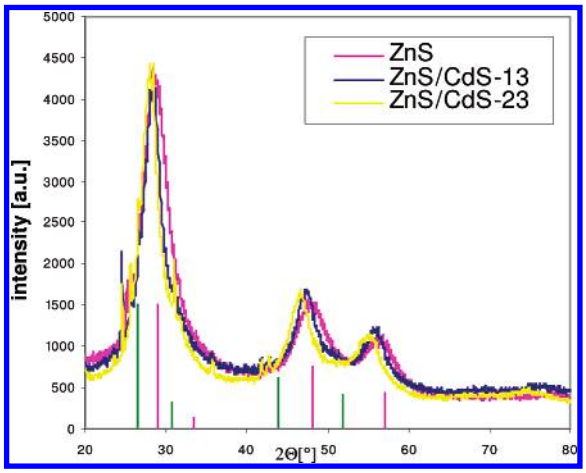

Figure 7. XRDs of the ZnS-core, the ZnS/CdS-13 system, and the ZnS/CdS-23 system.

capping layer (e.g., ZnS/CdS-21 compared with ZnS/CdS-23) is slightly more complicated to explain since even bulk ZnS does not absorb at energies lower than 3.7 eV. This behavior has also been observed earlier in the analogous CdS/HgS-system. It can be explained by an energetically more favorable relaxation of the wave functions of electron and hole with increasing thickness of the capping layer. The degree of shift is also in good agreement with the calculations.

The dotted lines in Figure 6 reflect the emission of the ZnS/CdS-13 and ZnS/CdS-23 samples recorded at 20 K. At room temperature, the samples did not reveal a detectable band gap emission and only a "trapped" emission at lower energies could be observed. This "trapped" emission increases in intensity with decreasing temperature and the band gap emission arises at approximately 50 K and increases with decreasing temperature. At 20 K a large "trapped" emission is observed at lower energies which may be due to stacking faults at the layer interfaces because of the lattice mismatch of approximately 8% between ZnS and CdS or by surface states, since pure ZnS nanocrystals show a comparable emission at slightly higher energy. The samples with less than three cladding layers of ZnS did not show any detectable band gap emission, supposedly because of a higher probability of presence of the charge carriers at the particle surface.

Powder X-ray Diffractometry (XRD). Figure 7 shows the XRD of the ZnS nanocrystals, the ZnS/CdS-13 and the ZnS/CdS-23 systems. The vertical bars show the bulk reflexes of cubic ZnS (pink lines) and CdS (green lines). The reflex position of the diffractogram for the pure ZnS sample corresponds very well with the bulk cubic ZnS structure; thus, the nanocrystals have cubic structure. The size of the nanocrystals can be calculated from the full width at half-maximum of the 111-reflex yielding a diameter of 3.0 nm (using the Debye−Scherrer equation and assuming defect-free crystals). The diffractograms of the ZnS/CdS-13 and ZnS/CdS-23 samples correspond to nanocrystals of a diameter of approximately 4.5 nm for both samples. The idealized structures have diameters of 4.8 nm (ZnS/CdS-13) and 5.1 nm (ZnS/CdS-23), the mismatch in the value obtained by the XRDs may be caused by an increasing amount of defects within the crystal structure with increasing thickness of the embedded CdS layer. Also, no indication for separate CdS particles being formed as a byproduct of the reactions has been found. The small shift of the reflexes of the ZnS/CdS-13 and ZnS/CdS-23 systems toward smaller angles and thus toward the values of bulk CdS is not fully understood so far. This may be due to the intermixing of ZnS and CdS in the nanocrystals as well as an additional lattice tension in the nanocrystals because of the incorporation of the very thin CdS layer.

Summary

Multilayered spherical CdS/HgS nanocrystals consisting of two embedded HgS layers in CdS and multilayered ZnS/CdS nanocrystals with one embedded CdS layer in ZnS have been prepared and were characterized by optical spectroscopy, XRD, and TEM. The results obtained are in good agreement with the postulated structures. Specifically, it could be shown that the simple "particle in the box" model with the effective mass approximation first used by Brus et al.[23] to describe the size quantization effect and later by Schooss et al.[13] to describe the CdS/HgS QDQWs is capable of describing even more complicated structures such as the presented CdS/HgS systems as well as multilayered structures made of other materials (ZnS/CdS).

Acknowledgment. This work has been supported by DIP-D3.1 "Functional Nanoparticle Architecture". We wish to thank S. Hickey for fruitful discussions concerning the manuscript.

References and Notes

(1) Spanhel, L.; Haase, M.; Weller, H.; Henglein, A. *J. Am. Chem. Soc.* **1987**, *109*, 5649.

(2) Peng, X.; Schlamp, M. C.; Kadavanich, A. V.; Alivisatos, A. P. *J. Am. Chem. Soc.* **1997**, *119*, 7019.

(3) Eychmüller, A.; Mews, A.; Weller, H. *Chem. Phys. Lett.* **1993**, *208*, 59.

(4) Mews, A.; Eychmüller, A.; Giersig, M.; Schooss, D.; Weller, H. *J. Phys. Chem.* **1994**, *98*, 934.

(5) Porteanu, H. E.; Lifshitz, E.; Pflughoefft, M.; Eychmüller, A.; Weller, H. *Phys. Status Solidi B* **2001**, *226*, 219.

(6) Eychmüller, A.; Voβmeyer, T.; Mews, A.; Weller, H. *J. Lumin.* **1994**, *58*, 223.

(7) Kamalov, V. F.; Little, R.; Logunov, S. L.; El-Sayed, M. A. *J. Phys. Chem.* **1996**, *100*, 6381.
(8) Little, R. B.; Burda, C.; Link, S.; Logunov, S.; El-Sayed, M. A. *J. Phys. Chem. A* **1998**, *102*, 6581.
(9) Yeh, A. T.; Cerrulo, G.; Banin, U.; Mews, A.; Alivisatos, A. P.; Shank, C. V. *Phys. Rev. B* **1999**, *59*, 4973.
(10) Braun, M.; Burda, C.; Mohamed, M.; El-Sayed, M. *Phys. Rev. B* **2001**, *64*, 035317.
(11) Koberling, F.; Mews, A.; Basché, T. *Phys. Rev. B* **1999**, *60*, 1921.
(12) Mews, A.; Kadavanich, A. V.; Banin, U.; Alivisatos, A. P. *Phys. Rev. B* **1996**, *53*, 13242.
(13) Schooss, D.; Mews, A.; Eychmüller, A.; Weller, H. *Phys. Rev. B* **1994**, *49*, 17072.
(14) Bryant, G. W. *Phys. Rev. B* **1995**, *52*, R16997.
(15) Jaskolski, W.; Bryant, G. W. *Phys. Rev. B* **1998**, *57*, R4237.
(16) Perez-Conde, J.; Bhattacharjee, A. K. *Phys. Status Solidi B* **2001**, *229*, 485.
(17) Little, R. B.; El-Sayed, M. A.; Bryant, G.; Burke, S. *J. Chem. Phys*. **2001**, *114*, 1813.
(18) Bryant, G. W.; Jaskolski, W. *Phys. Status Solidi B* **2001**, *224*, 751.
(19) Braun, M.; Burda, C.; El-Sayed, M. A. *J. Phys. Chem. A* **2001**, *105*, 5548.
(20) Dorfs, D.; Eychmüller, A. *Nano Lett*. **2001**, *1*, 663.
(21) Borchert, H.; Dorfs, D.; McGinley, C.; Adam, S.; Möller, T.; Weller, H.; Eychmüller, A. *J. Phys. Chem. B* **2003**, *107*, 7486.
(22) Chang, K.; Xia, J.-B. *Phys. Rev. B* **1998**, *57*, 9780.
(23) Brus, L. E. *J. Chem. Phys*. **1983**, *79*(11), 5566.
(24) Lifshitz, E.; Porteanu, H.; Glozman, A.; Weller, H.; Pflughoefft, M.; Eychmüller, A. *J. Phys. Chem. B* **1999**, *103*, 6875.